NANO · MICRO small
www.small-journal.com

Spatial Heterodyne Offset Raman Spectroscopy Enabling Rapid, High Sensitivity Characterization of Materials' Interfaces

*Han Cui, Andrew Glidle, and Jonathan M. Cooper**

Spatially offset Raman spectroscopy is integrated with a fiber-coupled spatial heterodyne spectrometer to collect Raman spectra from deep within opaque or scattering materials. The method, named spatial heterodyne offset Raman spectroscopy generates a wavenumber-dependent spatial phase shift of the optical signal as a "spectral" image on a charge-coupled device detector. The image can be readily processed from the spatial domain using a single, simple, and "on-the-fly" Fourier transform to generate Raman spectra, in the frequency domain. By collecting all of the spatially offset Raman scattered photons that pass through the microscope's collection objective lens, the methodology gives an improvement in the Raman sensitivity by an order of magnitude. The instrumentation is both mechanically robust and "movement-free," which when coupled with the associated advantages of highly efficient signal collection and ease of data processing, enables rapid interfacial analysis of complex constructs based on established biomaterials models.

1. Introduction

Raman spectroscopy is a well-established analytical method in which a "fingerprint spectra" resulting from the specific molecular signals of different components in a material can be used as a label-free and non-invasive imaging technique.[1,2] It has already been extensively used in industrial quality control and materials science research, including in particular biomaterials characterization (e.g., in regenerative medicine or tissue engineering to explore stem cell differentiation,[3] the biomolecular assessment of tissue engineering constructs,[4] and local heterogeneities in native and engineered materials[5]).

A current, existing deficiency of "traditional" Raman microspectroscopy when probing solid and complex samples, is its shallow penetration depth. Typically this is only several hundred micrometers in opaque or heavily scattering samples (the penetration depth is determined by the magnitude of both the excitation laser light at a certain depth and the ability of the microspectroscopy instrumentation to detect the resultant Raman scattered photons within a reasonable timescale). For example, in biomaterials research, the assessment of molecular and structural features below the surface of tissue remains a significant challenge.[6]

To address this, Pavel Matousek et al. proposed spatially offset Raman spectroscopy (SORS)[7] as a method that could greatly extend the analysis depth compared to traditional Raman measurements.[8] In traditional Raman microspectroscopy the Raman signal comes from scattering centers that are predominantly along the optical axis (i.e., those that are close to the axis of the microscope objective used to focus the incident laser beam). In contrast, in SORS the Raman scattered photons are predominantly collected from off-axis scattering centers (hence the term "offset"). The technique enables the collection of spectra containing molecular information with greater contributions from centers that are further from the surface of the material, that is, providing a greater penetration depth. This attractive feature of being able to probe the composition and structure of features buried deeply within a material, has already found applications in biomedicine, defense and security, industrial quality assurance, and cultural heritage research.[9–11] Nevertheless, there have been significant challenges in establishing experimental SORS configurations that are both easy to use and efficient in both the collection of photons and their processing. In particular, there are often technical obstacles associated with configuring the motion of optical elements to make measurements at different offset settings which, together with the low signal throughput and, in some instances, complex data processing, makes routine SORS measurement difficult.

As a consequence, a number of different variants of the SORS technique have emerged,[12–15] including fiber-based SORS, digital micromirror device (DMD)-based SORS (with discrete and continuous offset patterns), wavelength modulated

Dr. H. Cui
Beijing Key Lab for Precision Optoelectronic Measurement Instrument and Technology
School of Optics and Photonics
Beijing Institute of Technology
Beijing 100081, China
Dr. H. Cui, Dr. A. Glidle, Prof. J. M. Cooper
Division of Biomedical Engineering
James Watt School of Engineering
University of Glasgow
Glasgow G12 8LT, UK
E-mail: Jon.Cooper@glasgow.ac.uk

The ORCID identification number(s) for the author(s) of this article can be found under https://doi.org/10.1002/smll.202101114.

DOI: 10.1002/smll.202101114

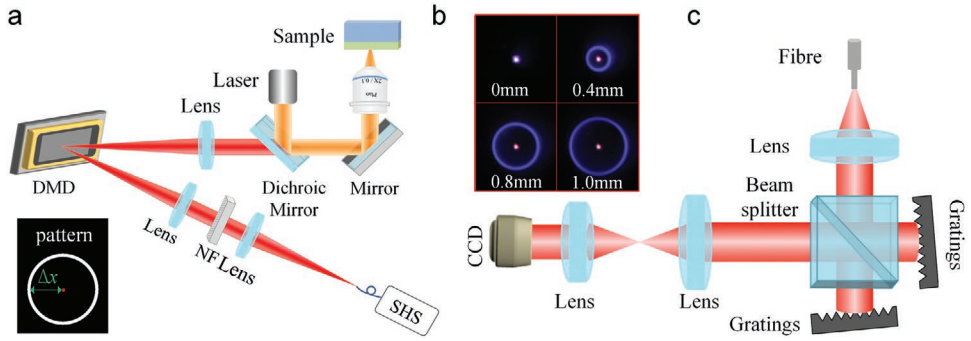

Figure 1. SHORS system. a) Schematic of SHORS; b)the relative position of laser spot (pink) and the pattern (purple) on DMD at different offset values, 0, 0.4, 0.8, and 1.0 mm; c) the principle of SHS.

SORS, and SORS using custom machined optical lenses. However, with many of these innovations, the need for sophisticated data processing has remained, particularly in systems such as those based upon DMDs (where, although the physical movement of large optical elements to make measurements at different offsets has been eliminated, the challenge has instead been translated to an increased complexity in signal processing). In particular, manipulating the SORS images collected on a charge-coupled device (CCD) based detector to extract high resolution spectra is a significant computational challenge (in part due to the low signal levels found in Raman spectra).

To overcome this, we incorporate a spatial heterodyne spectrometer (SHS) into our microscope, creating an instrument that is analogous to a Michelson interferometer based spectrometer.[16,17] In recent years, high resolution SHS systems have attracted attention due to them offering better light collection compared to similarly high resolution dispersive spectrometers.[18] Advantages and disadvantages of SHS systems are also associated with the distribution of "noise" across the spectrum (c.f. Fellgett's and Jacquinot's advantages when considering FTIR vs grating IR spectrometers). However, although SHS systems have better light collecting and SNR properties, there do exist some reflection losses on both the internal beamsplitter and gratings. Nevertheless, SHS have recently been effectively used in low-light and Raman applications[19] including when using ultraviolet laser sources for Raman,[20] collection of remote (or stand-off) Raman signals,[21,22] and biological analyses[20–23] (in both backscattering and transmission modes).[18,24] SHS configurations have also enabled instruments to be miniaturized,[25] as well as being used in hyperspectral[26] and Echelle grating–mirror[27] configurations. Whilst each of these have provided important incremental advances in Raman, to date SHS has not been used in combination with SORS to overcome current fundamental issues associated with its sensitivity, the speed of spectral acquisition and ease of data processing.

In the work reported here, we now describe how, by focusing the light from all of the mirrors in the DMD pattern of a SORS microscope onto the entrance of a single, large multimode optical fiber, we are able to couple a DMD-based system into an SHS having a high etendue. This results in an output in which no spectral corrections are needed, both greatly simplifying the data and/or signal processing tasks as well as increasing the signal collection efficiency, when compared to established SORS instruments. The resulting instrument, termed spatial heterodyne offset Raman spectroscopy (SHORS) integrates SHS and DMD-based SORS combining the "motion free" and high etendue features of SHS with its large aperture, so enabling us to collect spectra from all of the individual mirrors in an offset pattern formed on the DMD array, simultaneously, within a single acquisition.

The high signal collection efficiency of SHORS measurements, coupled with the large etendue enables high throughput acquisitions in which the signal/noise can be improved by an order of magnitude, compared to similar measurements made with a traditional dispersive spectrometer based DMD-SORS system. Finally, we note that all of the optical elements within the SHORS system are motionless, making the system much more reliable, repeatable, and, as a consequence of its compact and robust construction, having the potential of creating an instrument integrated into a small footprint (e.g., as a portable tool).

2. Results and Discussion

2.1. Spatial Heterodyne Offset Raman

We based the construction of our SHORS system around a DMD-based SORS arrangement, as shown in **Figure 1**a, where offset value can be controlled by the radius Δx of the pattern (more detail concerning the theory and analysis of DMD-based SORS systems are described in previous studies[15,28]). By placing a simple webcam at the sample position, we show the optical alignment of the system relative to the position of a laser spot (pink) and the image (purple) created by illuminating the DMD with white light (via the optical fiber that would normally be connected to the SHS), for the different DMD patterns associated with offset values, 0, 0.4, 0.8, and 1.0 mm, Figure 1b. Note, that when the offset value is 0 mm, the instrument works as a confocal Raman system. A single set of positioning adjustments of the other optical elements in Figure 1a required to achieve all of the images of Figure 1b, provide assurance that the laser and DMD patterns remain co-axially aligned for each different offsets without the need for further mechanical adjustments.

Figure 1c shows how the Michelson interferometer[16,17] concept is implemented in an SHS system; here, the two beams are split by the beamsplitter and strike diffraction gratings, rather than moving mirrors (as is generally found in FTIR

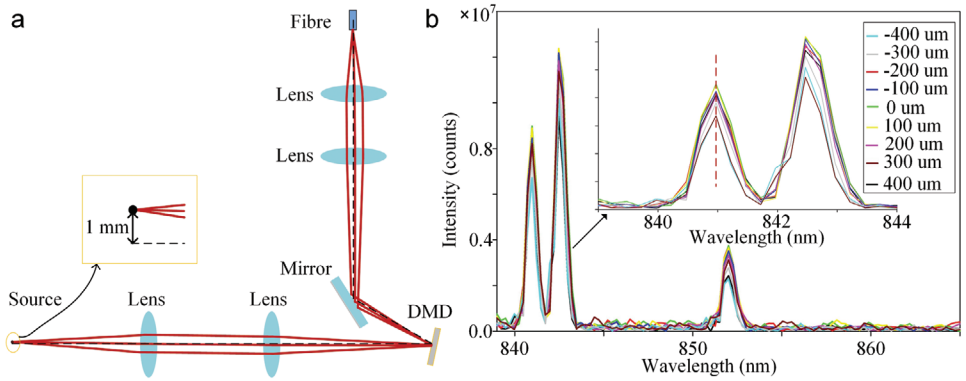

Figure 2. SHORS ability measurements. a) Simulation of the light path; b) the wavelength effect.

instrumentation). When these gratings are tilted, the generated wavefronts interfere, leading to a wavenumber-dependent spatial phase shift in the pattern captured as an image on the CCD detector. As a result, the SHS translates the spectrum from the spatial frequency domain to a temporal frequency domain. The Raman spectrum can subsequently be obtained SHS by applying a simple Fourier transform of the CCD image. All elements in the system are motionless during this process, making the system highly reliable, repeatable, and robust.

2.2. SHORS Can Perform SORS

For dispersive spectrometer based SORS, the entrance slit to the spectrometer either needs to be set to a large opening in order to collect offset spectra when using a pattern on a DMD array, or configured to accept a large fiber bundle spread out as a linear array at the spectrometer input. In contrast, in a SHORS instrument, there is no slit (nor indeed, need for one) at the input to the optical system. Thus, for a fiber coupled SHS system, maximal collection of light going into the fiber is the key to ensure the offset spectra are optimally captured.

To determine the optimal lens to converge the Raman scattered light reflected from the DMD array and direct it into the SHS fiber, we used OpticalRay Tracer (Version: 9.6, copyright by P. Lutus) to simulate various light paths (**Figure 2**a). As the inset to Figure 2a shows, light emanating from a point source positioned 1 mm away from the central axis of the optical system (dashed line) which mimics spectra from a DMD pattern corresponding to 1 mm offset measurements readily enters the aperture of a 910 µm optical fiber aperture (the lenses selected to achieve this here were 100, 125, 150, and 40 mm focal length).

With this novel application of a fiber coupled configuration, it is important to evaluate whether or not spectroscopically identical measurements are obtained for light reflecting from each of the DMD mirrors located at different positions in a given offset pattern when the light is focused into the coupling fiber. For example, when using a fixed configuration to focus the light reflected from the DMD into the fiber, light from mirrors in a 0.1 mm offset pattern will enter the fiber at a spatially different position compared to light from a 1 mm offset pattern. For this novel SORS configuration to be proven, there must be no wavelength shifts between spectra recorded for these two offset settings. Thus, to verify that the spectrum obtained from the SHS spectrometer is independent of the point at which the light enters the multimode input fiber, a spectral line from an Ar calibration lamp (Spectral Calibration Lamp, Argon, 6030, Newport) of minimal spatial size, was injected into different positions at the end of the 910 µm fiber.

Here, a spatially well-confined source was made by coupling the calibration lamp into a single mode fiber, the output of which was held in an x–y stage so as to inject light from the lamp to the different places on input face of the 910 µm coupling fiber. The spectra obtained when the single mode fiber traverses the input to the 910 µm coupling fiber in 100 µm steps are shown in Figure 2b. These clearly show that the spectral peaks are reported at a constant value (within the resolution limits of the SHS instrument) for all positions of the single mode fiber. This demonstrates that a fiber coupled SHORS configuration can be used to obtain offset spectra with the correct associated Raman shifts, without the additional signal processing corresponding to the reflection of offset Raman signals from different mirrors in the DMD patterns.

2.3. Advantages of Minimal Data Processing

As indicated above, a significant improvement of the SHORS system, when compared with dispersive spectrometer based DMD-SORS, is that no additional complex data processing is required to extract a spectrum from the collected data. For example, for traditional SORS based measurements, the assignment of spectral peaks acquired from a particular circular or semi-circular pattern set on the DMD (or a bundle of fibers) is a curve on the CCD array (**Figure 3**), corresponding to the reflected light from different parts of the DMD pattern entering the wide slit of the spectrometer at different angles (and leading to the appearance of a small wavelength shift in spectra coming from different parts of the DMD pattern). The small spectral shift necessitates manipulating the data from the CCD on a row-by-row basis so as to align the peaks from different rows and so obtain a high-resolution Raman spectrum.

In dispersive grating systems, such data manipulations required to eliminate this shift involves a series of steps that involve finding a formula fitting for the locus of the strongest spectral peaks, translating the spectra in each row to align

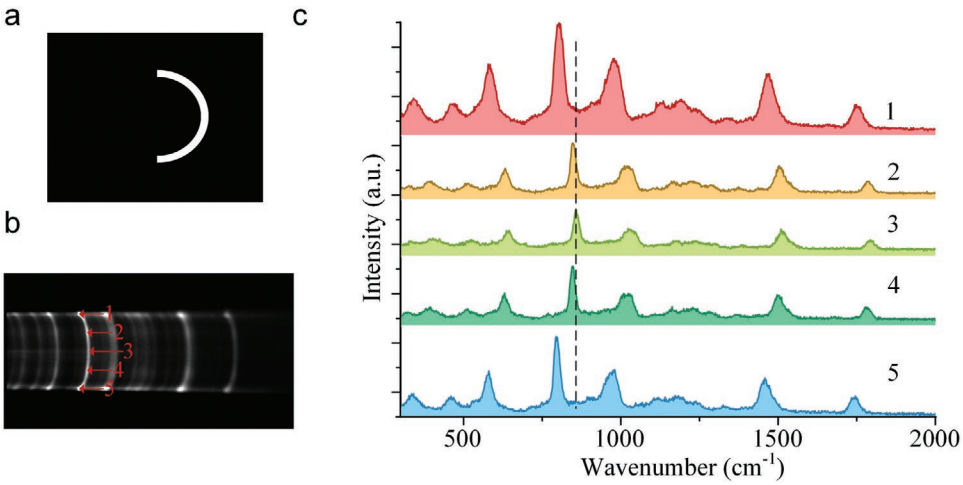

Figure 3. a) Wavelength shift pattern of "on" mirrors on DMD corresponding to a SORS offset of 2 mm. b) intensity pattern formed on spectrometer CCD corresponding to DMD mirror pattern of (a). c) Spectra extracting from each strip in (b) according to the horizontal strip positions labeled in (b).

the peaks into a series of vertical lines (i.e., transforming the detector image of Figure 3b so that, for example, the peaks at ca. 800 cm^{-1} in each of the strip spectra of Figure 3c are aligned with the dotted vertical line), summing the data in each of the CCD columns and then finally, correcting the spectral position to compensate for translating the individual rows. This procedure has to be performed for each offset pattern used.

Several drawbacks can be seen from this process, including deriving the formula for the detector image transformation when different patterns are used. Such formulae are complex non-linear functions of the detector pixel row and column index as well as being different the particular DMD pattern; simplifying this complexity reduces both the resolution and accuracy of the extracted spectra. Thus, it is difficult to obtain an accurate locus formula when the offset is small due to the small image on the detector, and, when the spectral intensities are weak (as with large offset patterns), there is a loss of precision in defining the locus of spectral peaks. These shortcomings around data processing are well-recognized as challenges within the SORS field,[28] and significantly decrease the flexibility, accuracy, and efficiency of the technique, when compared to the simplicity of one-shot data processing from a conventional Raman spectrometer that users are familiar with.

However, in contrast, when using a high etendue, interferometer based SHS system, rather than recovering the spectrum by manipulating different parts of a CCD image, SHORS is able to take a simple Fourier transform of the whole CCD image to obtain the spectrum. Thus, the SHORS Raman spectrum can be readily displayed in real time, without additional data processing. This real time display facility is of remarkable benefit and convenience when collecting either survey data or performing lengthy acquisitions from different parts of structures with complex internal (or external) topographies.

2.4. High Throughput Raman Performance

A second advantage of our fiber coupled SHORS is that measurements can be made at a much higher throughput, when compared to the DMD-SORS configurations used previously. For example, in previously reported DMD configurations, it was necessary to use semi-circular DMD patterns to avoid crosstalk and line broadening of the images collected on the dispersive spectrometer CCD.[28] The obvious consequence of using such a semi-circular DMD patters is that, for a given offset pattern, only half of the backscattered Raman light that is focused onto the DMD array, entering the spectrometer.

In contrast, when using the fibre-coupled SHS spectrometer, it is possible to use a full circle DMD pattern to reflect all of the offset Raman signal into the SHS coupling fiber (see Figure S1, Supporting Information), so doubling the number of photons acquired. In order to demonstrate this signal advantage, we collected model spectra from a specimen of uncoated paracetamol. Two groups of experiments were conducted, one using the DMD with a dispersive spectrometer, and the other using the SHORS system. First, for both spectrometers, conventional Raman measurements were made with no offset pattern loaded onto the DMD, that is, just a central, axial group of mirrors was switched "on" (here the system operates as a confocal Raman microscope). Measurements using the two spectrometers were made by simple changing the direction of the DMD mirror between measurements to avoid moving the sample and laser focusing objective.

To make a comparison between the dispersive spectrometer and SHS configurations, binning and electronic signal filtering parameters for the detectors were set to the same values and an efficient dispersive spectrometer grating was used that had a spectral resolution comparable to that of the SHS spectrometer. As **Figure 4**a shows, the spectrum from the dispersive spectrometer SORS (orange) is generally nosier than that from the SHORS system (blue) following a 30 s acquisition. Calculations made by taking the region between 1700 and 2000 cm^{-1} in the spectrum as a "flat" baseline region from which a figure of merit for "noise" can be extracted and the 1320 cm^{-1} peak intensity as a figure for the "signal" indicates that the SNR of the dispersive spectrometer SORS system is ≈11 while that of the SHORS system is around ≈104, giving an improvement in sensitivity of approximately an order of magnitude for this small offset.

The second group of SORS measurements made using the standard sample involved DMD patterns corresponds

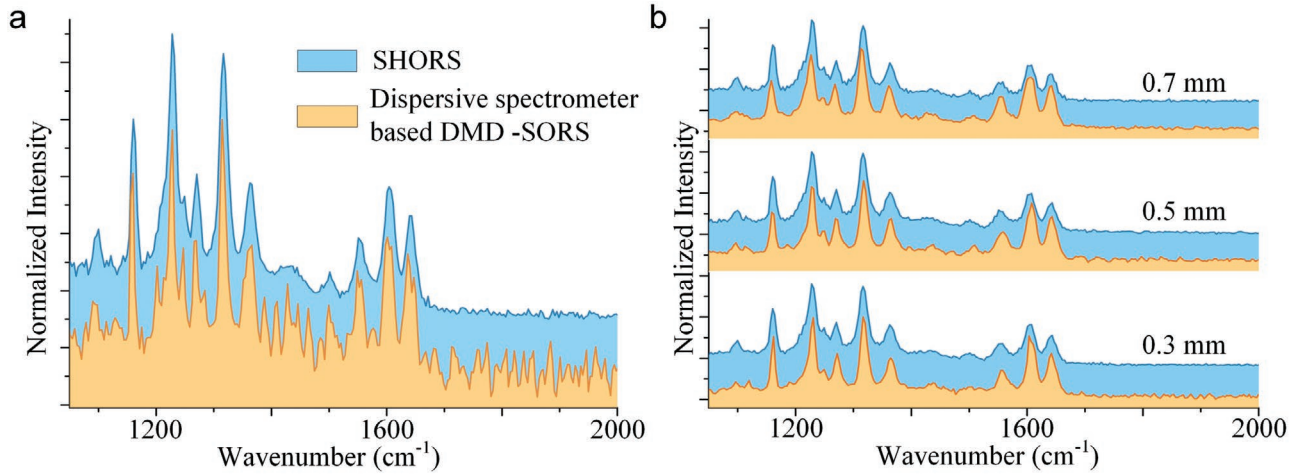

Figure 4. SNR comparison between SHORS and dispersive spectrometer SORS. a) Conventional Raman comparison, no offset applied. b) Offset spectra comparison between SHORS (blue) and dispersive spectrometer based DMD-SORS (orange), the offset spectra were recorded at spatial offset with 0.3, 0.5, and 0.7 mm, 30 s integration time and 16 accumulations for each test. Note, for clarity, the intensity scale for the SHORS measurements has been displaced upward to avoid overlap of the SHORS and DMD-SHORS traces.

to offset values of 0.3, 0.5, and 0.7 mm. Here it was necessary to use a fully open slit on the dispersive spectrometer and thus larger signals were captured (Figure 4b). Nevertheless, the improvement in SNR for the SHORS system was, again, an order of magnitude better for these offset spectra. This higher SNR not only improves the detectability of signals in a SHORS system, but also makes it more possible to do SORS measurements on a shorter timescale. To demonstrate this latter advantage, experiments were performed with offsets ranging from 0 to 1 mm to discover the acquisition time required by a SHORS configuration to obtain a similar SNR signal as that obtained after 30 s from a dispersive spectrometer based DMD-SORS system (**Table 1**). Thus the results of Table 1 indicate that the throughput of SHORS can be at least 30 times more than that of a dispersive spectrometer SORS system. These experimental results contrast with some of the predictions made following the simulations of Luca et al.[29] and maybe a consequence of the scattering factors used in those simulations and/or the improved optical collection realized here.

Table 1. Time comparison to reach same SNR.

Offset [mm]	Dispersive spectrometer based DMD-SORS integration time [s]	SNR	SHORS integration time [s]	SNR
0.0	30	11.3	0.5	11.6
0.1	30	9.7	0.4	9.9
0.2	30	9.9	0.3	10.2
0.3	30	10.6	0.2	10.8
0.4	30	10.0	0.25	9.6
0.5	30	9.7	0.3	10.3
0.6	30	9.4	0.25	10.4
0.7	30	9.1	0.3	9.7
0.8	30	9.7	0.4	10.0
0.9	30	11.0	0.6	10.7
1.0	30	11.7	1.0	11.9

Note: Table 1 gives details of data integration time required in order to collect SHORS spectra having a similar SNR to those collected when acquiring data for 30 s using a dispersive spectrometer.

2.5. Biomaterial Models

Here, we used two phantom models to examine the influence of different aspects of the soft tissue phantoms on the collected SHORS spectrum. In the first model, nanometer sized TiO_2 particles were added to a polydimethylsiloxane (PDMS) matrix to simulate scattering centers, as used before.[30] **Figure 5**a shows how the bone/tissue phantom was constructed, with the depth, *d*, between the surface of the tissue phantom and the center of the bone sample being adjustable between different samples.

A series of measurements were performed with offset values from 0.0 to 1.0 mm with the results for the instance of a 2 mm ($d = 4$ mm) thick tissue phantom being shown in Figure 5b. As expected, the peaks at ≈1410 and ≈1260 cm^{-1} due to the bending of CH_3 bonds and C—O stretches in PDMS[31] are shown in all the offset spectra, with the peaks at ≈960 cm^{-1} (hydroxyapatite (HAP)[32]) and ≈1070 cm^{-1} (carbonate[33]) increasing in relative intensity (to the strongest band) as the offset increases. As with other SORS measurements on similar material systems, the changes in the relative intensities of the Raman bands of HAP (960 cm^{-1}) and CH_3 bonds from PDMS (1410 cm^{-1}) vary with the spatial offset in a close to linear fashion (Figure 5c).

Measurements with other thicknesses of TiO_2-PDMS tissue phantom indicated that it was necessary to increase the thickness to ≈6 mm ($d = 8$ mm) before the phosphate peak disappeared from all the offset spectra except of that corresponding to a 1.0 mm offset, that is, the maximum analysis depth that can be achieved with the collection lens, DMD, and coupling fiber used here is 4–6 mm.

Following this validation of the SHORS technique for a simple binary system, to examine the performance with hydrogel based soft tissue phantoms that are closer to those

used in actual regenerative medicine or tissue engineering studies, we used a 3D bovine serum albumin (BSA)-polyethylene glycol (PEG)-hydrogel scaffold (detailed in the 3D BSA-PEG hydrogel scaffold fabrication sub-section of Experimental section, below) instead of TiO_2-PDMS. Here, the bone phantom was located 2.5 mm away from the outer surface of the hydrogel scaffold due to the greater scattering of the BSA-PEG-hydrogel leading to a decrease in the phosphate signal relative to the scattering from the background matrix.

Again a series of measurements with spatial offsets from 0.0 to 1.0 mm were performed (**Figure 6**). These showed Raman bands at ≈1660 cm^{-1} (C=O stretch) and ≈1470 cm^{-1} (δ(CH2) deformation) from BSA[34] (the PEG hydrogel also contributes to the $\delta(CH_2)$ deformation band). The trend in the decrease and increase of peaks as the offset increases for this hydrogel phantom is similar to that seen for the construct of Figure 5b, that is, bands from the bone phantom (phosphate, carbonate, and CH_3 of PDMS) increase as the offset increases and those of the BSA and PEG decrease.

It is noted that in comparison with the spectra of the simpler phantom of Figure 5, the spectra for the hydrogel/BSA based phantoms are more noisy. This is likely to be due to the greater scattering from the BSA centers within the hydrogel at the high concentration of BSA used. In non-synthetic biological samples, for example, natural bone, these scattering centers will also be present and in their measurement, careful consideration should be given to the choice of laser wavelength being well matched with the detector sensitivity and window coating materials. Here, the use of a 780 nm wavelength source may not be best suited to the DU 888 detector used here when measuring the weakest of Raman signatures, and a detector with greater NIR sensitivity should be used (note, that the use of the EM feature in the 888 EMCCD did not improve the signal/background quality in this instance, although it was beneficial when performing measurements on samples that only had a small degree of background scattering, where the detector read-out noise was more significant). Future optimization of sources and sensors is likely to lead to further improvements in both sensitivity and consequently throughput with decreases in acquisition time. Nevertheless, this higher concentration is more representative of the general protein/DNA/lipid loading that might be found in studies involving real cell based biological samples.

3. Conclusion

We show that SHORS can be used as a high sensitivity, high throughput methodology for materials analysis, with simple

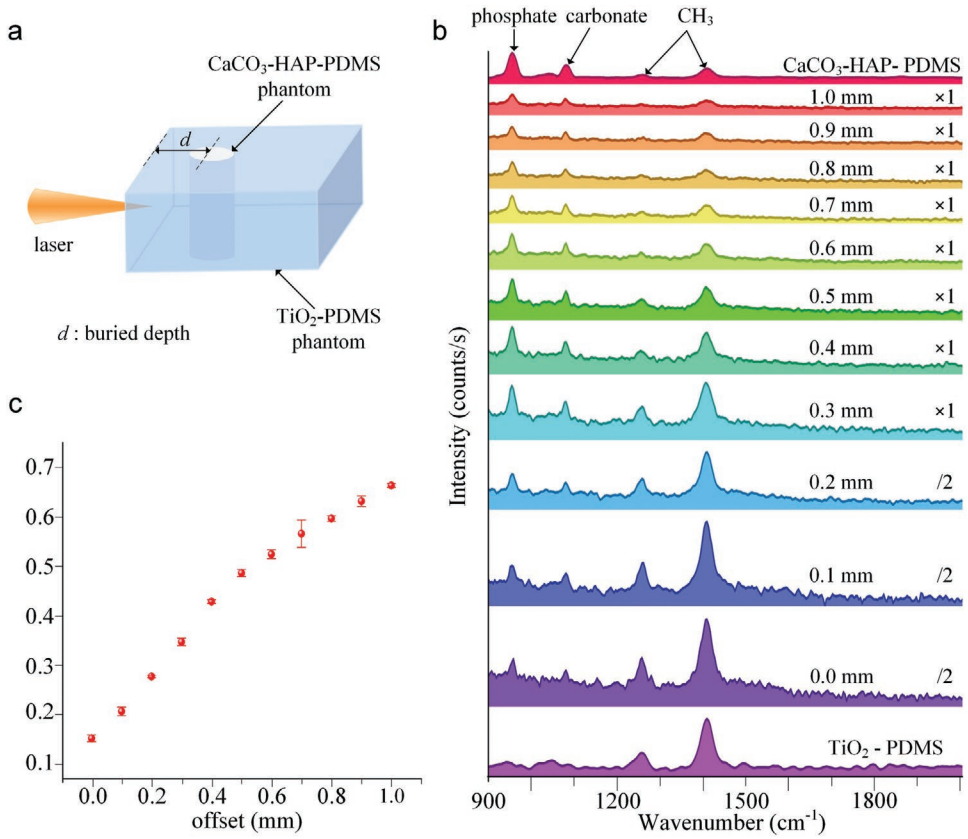

Figure 5. Phantom offset spectra test. a) Phantom sample consisting of tissue and bone phantom; b) offset spectra recorded at spatial offsets from 0.0 to 1.0 mm; spectra of TiO_2-PDMS and $CaCO_3$-HAP-PDMS phantom at the bottom and top of panel for reference, $d = 4$ mm. ×1 and/2 refer to scale factors applied to the spectrum intensity. c) The ratio of Raman band intensity at 960 and 1410 cm^{-1}. Ratios were obtained by integrating the area under the two peaks. No background subtractions have been applied.

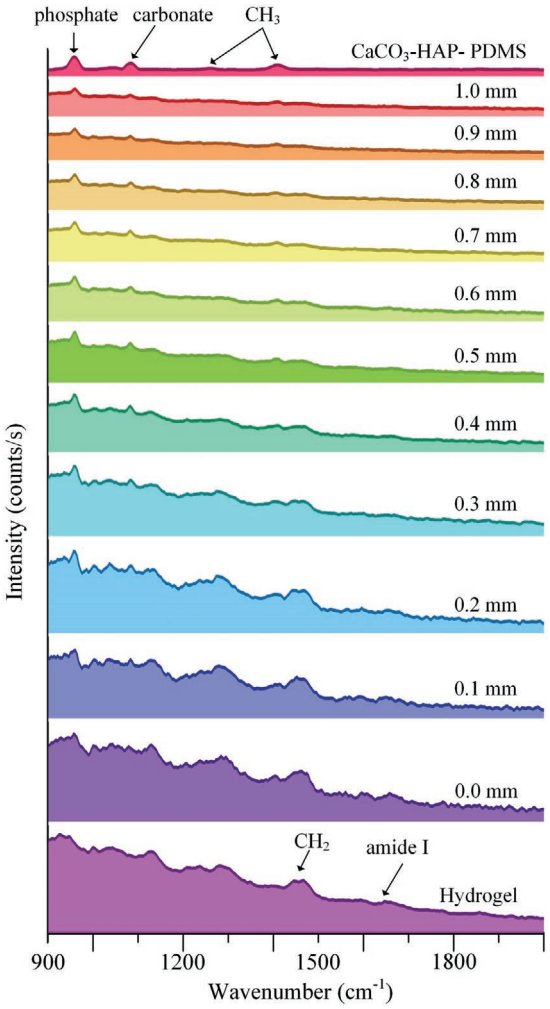

Figure 6. SORS measurements of BSA-PEG hydrogel with embedded bone phantom sample. Offset spectra recorded at spatial offset from 0.0 to 1.0 mm with the spectra of hydrogel and turbot bone at the bottom and top for reference, the front surface of bone phantom is 2.5 mm away from the hydrogel edge. No background subtractions have been applied.

data processing and "motionless" optics. By considering the SHS as a Michelson interferometer, with a beam splitter and diffraction gratings, we can produce a wavenumber-dependent spatial phase shift in the pattern captured as an image on the CCD detector. When used in conjunction with a DMD device to select the Raman scattered photons corresponding to a particular "offset," unlike with other experimental configurations, this fiber coupling method enables all of these offset scattered photons to be collected in a detector image that can be processed using a single transform.

The system has the advantages of being able to collect spatially resolved molecular profiles, whilst the use of the fiber coupling eliminates the extensive and often empirical data processing required to extract offset spectra. In addition, an order of magnitude improvement on SNR levels when compared with the dispersive spectrometer based SORS, provides future opportunities for SHORS possible to perform real-time detection or deep-Raman imaging.

4. Experimental Section

Spatial Heterodyne Offset Raman System: In the SHORS system constructed here, a 780 nm continuous wave laser (XTRA I, Toptica Photonics, Germany) was used as the excitation source which was reflected by a dichroic mirror (Di02-R785-25 × 36, Semrock, USA) and passed through a convex lens (LA1608-B-ML, Thorlabs, USA) so as to be focused on the sample. The SORS signal was collected by the same convex lens and focused onto a DMD using a 125 mm focal length lens. The DMD consisted of 912 × 1140 array micro-mirrors on a 7.6 µm pitch (DLP4500NIR, Texas Instruments). The offset value was set by simply placing different patterns on the DMD as a suitable bit mask within the LC 4500NIR controller (Keynote Photonics, USA). Finally, the reflected signal from the DMD mirror was focused into a multimode 910 µm diameter fiber, and so coupled into the SHS (IS-Instruments, UK) fitted with an EM-CCD detector (DU-888E, Andor, UK).

Data Processing: The spectra from SHORS were obtained directly using in-built Matlab routines (version 2016b, The MathWorks, USA), without the need for additional processing that was needed to apply wavelength corrections to different parts of the CCD image in a dispersive spectrometer based DMD-SORS configuration.[28]

In this study, two types of the biomaterials model phantoms were used, comprising either a polymer-based,[30] or a 3D hydrogel systems, as mimics/phantoms for soft and hard tissues, described below:

Polymer Based Soft Phantoms: In the first instance, PDMS was used to construct the bulk matrix[35] with nanometer size rutile titanium dioxide (TiO_2) particles, thereby simulating scattering centers in the soft tissue phantom.[36] It was found that a concentration of 0.75 mg mL^{-1} of TiO_2 led to a scattering coefficient of ≈1 mm^{-1},[35–37] analogous to that which might be found when making SORS measurements going through several mm of tissue. Again following earlier work,[30] the bone phantom was composed of calcium carbonate ($CaCO_3$) (Sigma Aldrich) and HAP (Sigma Aldrich) in a ratio of 1:3 w/w, based on previous study on apatite composition of bone and biomineral deposits in tissue.[30,38,39]This was mixed with uncured PDMS to give a concentration of 500 mg mL^{-1} of the mixed mineral powder. The two parts of PDMS kit (Sylgard 184 Silicone Elastomer Kit) were mixed in a ratio of 10:1 of base to curing agent. The TiO_2 particles (190 nm, TiONA 128, Tronox), were sifted through a 30 µm strainer (MACS SmartStrainers (30 µm)) to break up any clumped particles. This fine TiO_2 powder was added to the PDMS with stirring to make a homogeneous mix. The TiO_2-PDMS mixture was placed in a vacuum to degas for half an hour, and then left overnight at room temperature (25 °C) to cure thoroughly. To create the bone phantom, a 4 mm diameter by 9 mm height cylinder was extracted from a cured slab of the $CaCO_3$-HAP-PDMS material using a biopsy punch. This was then either inserted into a similarly made hole in the cured soft tissue phantom, or placed immediately behind a small slab of material (for instances where the material was too fragile to cut a hole in with a biopsy punch).

3D BSA-PEG Hydrogel Scaffold Fabrication: BSA-PEG hydrogels were prepared by adding BSA and a photo-initiator (Irgacure 2959, Sigma Aldrich) to a 4-Arm PEG-Acrylate (molecular weight: 10 kDa, Creative PEGWorks) solution. (n.b. BSA was used as an inexpensive "model" protein (molecular weight: 66 kDa, Sigma Aldrich) in this hydrogel scaffold rather than more costly therapeutic proteins). Hydrogel scaffolds were made by photopolymerisation of a solution comprising concentrations of 10% w/v PEG, 10% w/v BSA, and 0.05% w/v Irgacure 2959, in phosphate buffered saline (Sigma Aldrich). Again, the mixed solution was degassed in a vacuum before pouring into a 10 mm ×10 mm cuvette for irradiation with UV light (320–390 nm, 5 mW cm^{-2} with 10 min exposure on each face, in order to achieve the polymerization throughout the gel).

Supporting Information

Supporting Information is available from the Wiley Online Library or from the author.

Acknowledgements

The authors gratefully acknowledge the support of the Engineering and Physical Sciences Research Council (EP/P001114/1) and the National Centre for the Replacement, Refinement and Reduction of Animals in Research (CRACK IT Challenge 30: RaTS) as well as IS Instruments' assistance in establishing the technique.

Conflict of Interest

The authors declare no conflict of interest.

Data Availability Statement

The data that support the findings of this study are available from the authors on reasonable request.

Keywords

fibre coupled Raman Spectroscopy, high throughput SORS, on-the-fly SORS data processing, spatial heterodyne Raman spectroscopy, spatially offset Raman spectroscopy

Received: February 23, 2021
Revised: April 18, 2021
Published online: May 19, 2021

[1] C. V. Raman, K. S. Krishnan, *Nature* **1928**, *121*, 501.
[2] I. Notingher, L. L. Hench, *Expert Rev. Med. Devices* **2006**, *3*, 215.
[3] Y. Ilin, J. S. Choi, B. A. Harley, M. L. Kraft, *Anal. Chem.* **2015**, *87*, 11317.
[4] A. Kunstar, A. M. Leferink, P. I. Okagbare, M. D. Morris, B. J. Roessler, C. Otto, M. Karperien, C. A. Van Blitterswijk, L. Moroni, A. A. van Apeldoorn, *J. R. Soc., Interface* **2013**, *10*, 20130464.
[5] M. Albro, M. Bergholt, J. St-Pierre, A. V. Guitart, H. Zlotnick, E. Evita, M. Stevens, *npj Regener. Med.* **2018**, *3*, 3.
[6] C. M. Perlaki, Q. Liu, M. Lim, *Appl. Spectrosc. Rev.* **2014**, *49*, 513.
[7] P. Matousek, I. Clark, E. Draper, M. Morris, A. Goodship, N. Everall, M. Towrie, W. Finney, A. Parker, *Appl. Spectrosc.* **2005**, *59*, 393.
[8] P. Matousek, N. Stone, *J. Biophotonics* **2013**, *6*, 7.
[9] Y. Cho, S. W. Song, J. Sung, Y.-S. Jeong, C. R. Park, H. M. Kim, *Analyst* **2017**, *142*, 3613.
[10] D. Bersani, C. Conti, P. Matousek, F. Pozzi, P. Vandenabeele, *Anal. Methods* **2016**, *8*, 8395.
[11] B. Gardner, P. Matousek, N. Stone, *Anal. Chem.* **2019**, *91*, 10984.
[12] M. V. Schulmerich, W. F. Finney, R. A. Fredricks, M. D. Morris, *Appl. Spectrosc.* **2006**, *60*, 109.
[13] P. Matousek, *Appl. Spectrosc.* **2006**, *60*, 1341.
[14] M. Chen, J. Mas, L. H. Forbes, M. R. Andrews, K. Dholakia, *J. Biophotonics* **2018**, *11*, 201700129.
[15] H. Cui, A. Glidle, J. M. Cooper, *IEEE Access* **2020**, *8*, 62905.
[16] J. M. Harlander, F. L. Roesler, S. Chakrabarti, in *Proc. SPIE*, SPIE, San Diego **1990**.
[17] J. M. Harlander, *PhD Thesis*, The University of Wisconsin-Madison, **1991**.
[18] M. Foster, J. Storey, M. Zentile, *Opt. Express* **2017**, *25*, 1598.
[19] J. Harlander, R. J. Reynolds, F. L. Roesler, *Astrophys. J.* **1992**, *396*, 730.
[20] M. J. Egan, S. M. Angel, S. K. Sharma, *J. Raman Spectrosc.* **2017**, *48*, 1613.
[21] N. Lamsal, S. K. Sharma, T. E. Acosta, S. M. Angel, *Appl. Spectrosc.* **2016**, *70*, 666.
[22] M. J. Egan, T. E. Acosta-Maeda, S. M. Angel, S. K. Sharma, *J. Raman Spectrosc.* **2020**, *51*, 1794.
[23] G. Hu, W. Xiong, H. Luo, H. Shi, Z. Li, J. Shen, X. Fang, B. Xu, J. Zhang, *Appl. Spectrosc.* **2018**, *72*, 151.
[24] M. Foster, J. Storey, P. Stockwell, D. Widdup, *Opt. Express* **2015**, *23*, 3027.
[25] P. D. Barnett, S. M. Angel, *Appl. Spectrosc.* **2017**, *71*, 988.
[26] A. Allen, A. Waldron, J. M. Ottaway, J. C. Carter, S. M. Angel, *Appl. Spectrosc.* **2020**, *74*, 921.
[27] J. Qiu, X. Qi, X. Li, Z. Ma, Y. Tang, X. Mi, X. Zheng, R. Zhang, *Opt. Express* **2018**, *26*, 11994.
[28] Z. Liao, F. Sinjab, G. Gibson, M. Padgett, I. Notingher, *Opt. Express* **2016**, *24*, 12701.
[29] L. Ciaffoni, P. Matousek, W. Parker, E. McCormack, H. Mortimer, *Appl. Spectrosc.* **2020**, *75*, 241.
[30] I. E. I. Petterson, F. W. Esmonde-White, W. de Wilde, M. D. Morris, F. Ariese, *Analyst* **2015**, *140*, 2504.
[31] D. Cai, A. Neyer, R. Kuckuk, H. M. Heise, *J. Mol. Struct.* **2010**, *976*, 274.
[32] M. S. Bergholt, J.-P. St-Pierre, G. S. Offeddu, P. A. Parmar, M. B. Albro, J. L. Puetzer, M. L. Oyen, M. M. Stevens, *ACS Cent. Sci.* **2016**, *2*, 885.
[33] B. R. McCreadie, M. D. Morris, T.-c. Chen, D. S. Rao, W. F. Finney, E. Widjaja, S. A. Goldstein, *Bone* **2006**, *39*, 1190.
[34] A. Synytsya, P. Alexa, J. de Boer, M. Loewe, M. Moosburger, M. Würkner, K. Volka, *J. Raman Spectrosc.* **2007**, *38*, 1646.
[35] D. M. M. de Bruin, R. H. Bremmer, V. M. Kodach, R. de Kinkelder, J. van Marle, T. G. van Leeuwen, D. J. Faber, *J. Biomed. Opt.* **2010**, *15*, 025001.
[36] X. Bi-Tao, Z. Bao-Xue, B. Jing, Z. Qing, L. Yan-Biao, C. Wei-Min, C. Jun, *Chin. Phys. B* **2008**, *17*, 3713.
[37] A. Kim, B. C. Wilson, in *Optical-Thermal Response of Laser-Irradiated Tissue*, Springer, Berlin **2010**, p. 267.
[38] M. D. Morris, G. S. Mandair, *Clin. Orthop. Relat. Res.* **2011**, *469*, 2160.
[39] A. Carden, M. D. Morris, *J. Biomed. Opt.* **2000**, *5*, 259.